ELSEVIER

Polymer 42 (2001) 827–838

polymer

www.elsevier.nl/locate/polymer

Interrelationships between electrical and mechanical properties of a carbon black-filled ethylene–octene elastomer

L. Flandin, A. Hiltner*, E. Baer

Department of Macromolecular Science, and Center for Applied Polymer Research, Case Western Reserve University, Cleveland, OH 44106-7202, USA

Received 10 November 1999; received in revised form 19 February 2000; accepted 23 February 2000

Abstract

The mechanical and dc electrical properties of a carbon black-filled ethylene–octene elastomer (EO) are reported. The stress–strain curves of the composites, scaled with that of the unfilled polymer up to approximately 500% strain, suggest good filler–matrix adhesion. The large reinforcement effect of the filler followed the Guth model for non-spherical particles. Electrical behavior under large strain was divided in four qualitatively or quantitatively different regimes that differentiated carbon black composites with the EO matrix from carbon black composites with chemically vulcanized matrices. Among the most notable features of the EO composites was the completely reversible variation of the resistivity, up to 20% strain, suggesting that these materials might be useful as strain gauges. In addition, depending on the carbon black content, the composites retained low resistivity to high strains. From the results of various thermo-mechanical treatments, a microstructural model for the response to stretching was proposed. This model incorporated dynamic junctions specific to the EO matrix to describe the mechanical properties, the decrease in resistivity at low strains (20%), and the weak increase in resistivity at intermediate strains (up to about 300%).

Keywords: Ethylene–octene copolymer; Carbon black; Composites

1. Introduction

Low-resistivity elastomers typically employ vulcanized rubber as a matrix for dispersion of a large variety of fillers, mainly carbon blacks [1,2], carbon fibers [3] and metallic particles [4]. In addition to imparting conductivity, the filler generally improves environmental resistance and mechanical properties. As these composites do not always exhibit the best balance of properties, alternative elastomeric matrices are of interest.

In recent years, the development of Dow's INSITE™ constrained geometry catalyst technology has led to the production of a new class of elastomers based on homogeneous ethylene-α-olefin copolymers. In particular, copolymers with more than 8% octene possess low crystallinity and rubber-like behavior that depends on physical rather than chemical junctions [5]. The main advantage of these polymers over chemically vulcanized elastomers, lies in their ease of processing and post-processing, much like conventional polyethylenes. These elastomeric materials have been commercialized and are the subject of numerous investigations as unfilled polymers [6–8], however very little is known about their mechanical and electrical properties when reinforced with conducting fillers [9].

Electrical properties of binary mixtures depend strongly on the microstructure. In particular, dispersion state [10], filler geometry [11], and filler–filler [10] and filler–matrix [12] interactions strongly affect the electrical properties of composite materials. External variables, such as temperature [13,14] and mechanical stretching [15,16], can significantly affect the microstructure and thereby the macroscopic conductivity. If there is a simple relationship between electrical conductivity and an external variable, the composite has potential applications as a sensor. For these reasons, the development of new conductive composites requires an understanding of the changes in conductivity that might occur in service. Conversely, measurement of electrical conductivity under large strain can be a probe to understanding microstructural changes.

Recently, composites that incorporate a conductive filler into an ethylene–octene (EO) elastomer matrix were evaluated for electrical and mechanical properties [17]. Comparing three types of fillers (carbon fiber, high-structure carbon black, and low-structure carbon black), it was found

* Corresponding author. Tel.: +1-216-368-4186; Fax: +1-216-368-6329.

E-mail address: pah6@cwru.edu (A. Hiltner).

0032-3861/01/$ - see front matter
PII: S0032-3861(00)00324-4

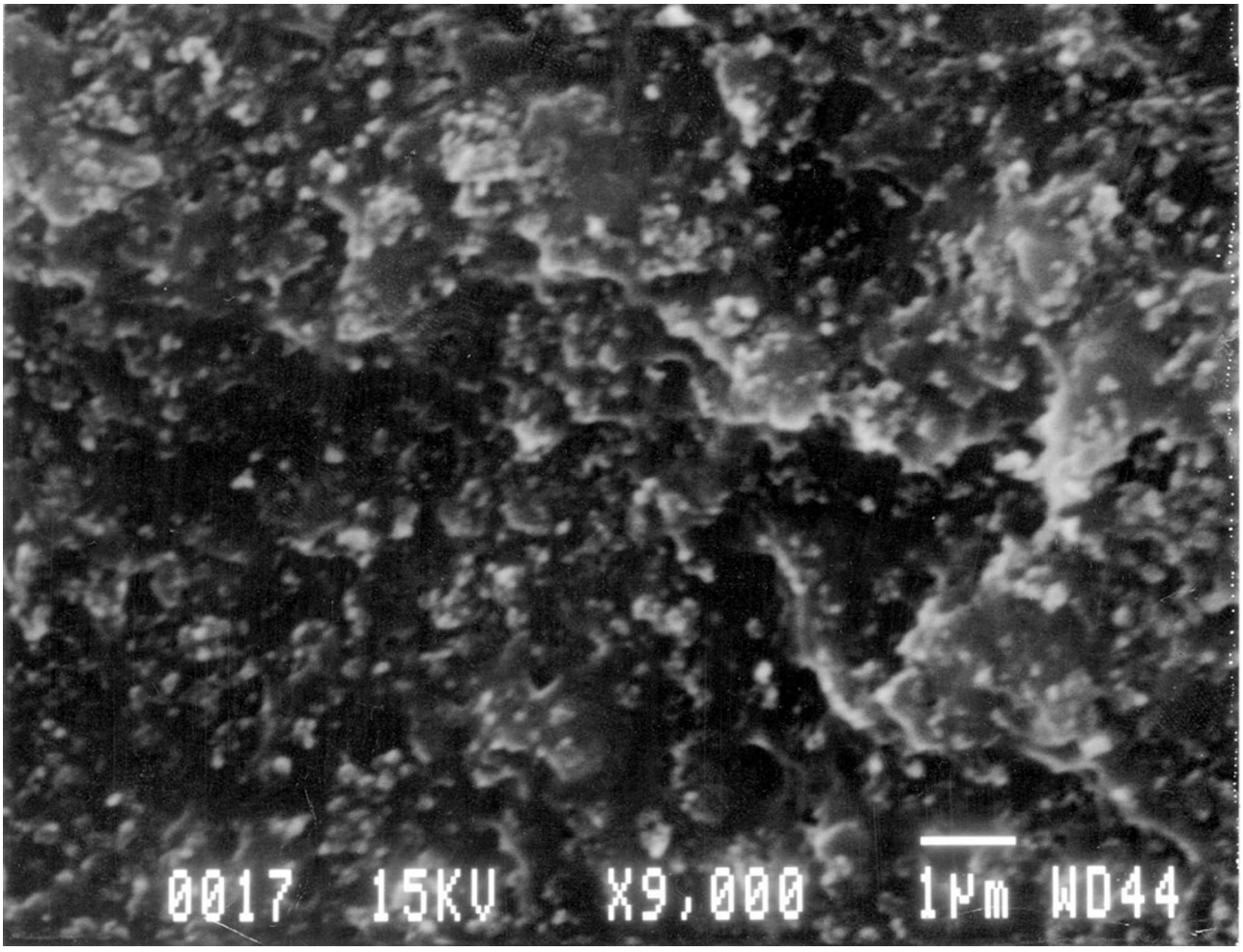

Fig. 1. Scanning electron micrograph of a cryofracture surface showing dispersion of the carbon black filler (20% v/v).

that the composite with high-structure carbon black exhibited some interesting electrical and mechanical characteristics. The present work examines, in more detail, the properties of EO with a high-structure carbon black filler. The mechanical behavior was studied as a function of filler content in order to quantify the reinforcement effect of the particles. However, the work focused primarily on in situ changes of resistivity during uniaxial stretching. Particular attention was paid to the occurrence of reversible and irreversible phenomena. The electrical and mechanical properties were analyzed for the purpose of correlating macroscopic behavior with microstructural events.

2. Materials and methods

2.1. Materials

An EO elastomer, synthesized by the Dow INSITE™ technology and commercialized under the designation DEG-8180, was the matrix in this study. The polymer had a density of 0.863 g/cc and behaved as an elastomer at room temperature [5]. A high-structure carbon black designated as Conductex 975 Ultra was supplied by the Columbian Chemicals Company (particle diameter 21 nm; dibutyl phthalate absorption number (DBPA) 170; surface area 242 m^2/g; volatiles 1%; mean aggregate size 110 nm; weight mean aggregate size 300 nm; average aspect ratio 2.78).

Blending was carried out in a Haake Rheomix 600 mixing head with a 44 cm^3 mixing volume. The polymer was melted in the mixing head for 1 min before the filler was slowly added. The total operation lasted 10 min, during which time the mixing head was maintained at 40 rpm and 200°C. All batches, as well as the unfilled elastomer, were processed under identical conditions. After cooling, the blends were compression molded into 2 mm thick plaques. The materials were sandwiched between Mylar® sheets, heated at 200°C under minimal pressure for 2 min, then subjected to repeated pressure-release cycles for 8 min to remove any air bubbles resulting from the mixing procedure. Plaques were rapidly cooled to ambient temperature under minimal pressure in a cold molder.

To confirm good particle dispersion, specimens were

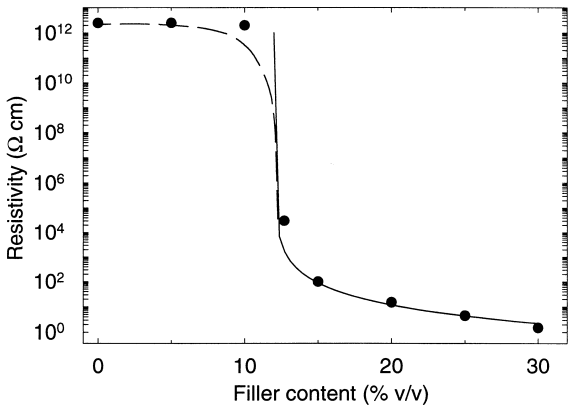

Fig. 2. Resistivity as a function of carbon black content. The solid line is the statistical percolation fit, Eq. (3).

broken in liquid nitrogen, coated with 10 nm of gold and observed in a JEOL JXA 840A instrument. Fig. 1 presents a micrograph of the cryofractured surface of a composite containing 20% (v/v) carbon black. Uniformly dispersed light spots represent carbon black particles. The particle size, in the range of 50–500 nm, is consistent with the primary aggregate size given by the manufacturer (weight mean aggregate size of 300 nm). The roughness of the fracture surface indicates good adhesion between the particles and the matrix.

2.2. Methods

Stress–strain behavior in uniaxial tension was measured at ambient temperature with ASTM 1708 microtensile specimens, cut from the compression molded plaques. The grip separation was 22.3 mm and included the fillet section, the specimen width was 4.8 mm. Specimens were deformed in an Instron 1123 testing machine at a rate of 20% min^{-1}, except when stipulated otherwise. Marks were drawn on the specimens to measure the draw ratio from a video recording.

Electrical properties were measured with a four-terminal technique using a Keithley model 220 as current source, and Keithley model 619 for voltage and current measurement, as described previously [17]. The device was interfaced to a computer to record data. The minimum time required to obtain a measurement was 0.12 s. The error in the measurements, determined with standard resistances, was less than 2% in the range 10^{-7}–10^{-2} A for current, and 10^{-5}–100 V for voltage.

To measure in situ the changes in conductivity upon stretching, strip-like specimens were used with an initial length of $L_0 = 135$, width of $W_0 = 10$, and thickness $H_0 = 2$ mm. For measurements along the specimen length (parallel direction), flat clamps covered with copper foil were used. The clamps applied an approximately constant pressure even on the strained specimens and, therefore, could be used to measure resistance during deformation up to fracture. The measured resistivity did not depend on the specimen geometry or the pressure applied to the electrodes, furthermore gold electrodes deposited on the cut edges of the specimen gave the same resistivity as electrodes applied to the molded surfaces. Therefore, the measured parallel resistivity was taken as a bulk value, although the possibility that it represented a surface resistivity cannot be absolutely eliminated.

For electrical measurements through the thickness (perpendicular direction), electrodes consisted of thick gold layers (≈ 200 nm) deposited on both surfaces. The specimen was mounted in the Instron and the stress σ, specimen length L, and voltage were recorded during uniaxial extension. The applied current was 10^5A unless, at higher strains, the voltage approached the limits of the device, in which case the current was decreased. When this occurred, the resistance changed very slightly indicating that deformation did not alter the ohmic behavior.

The resistivity was obtained from the measured resistance R and the geometrical changes in the specimen. The constant volume assumption, i.e. Poisson's ratio equal to 0.5, is generally considered valid for polymers above the glass transition temperature. With this assumption, the resistivities parallel and perpendicular to the extension direction were, respectively, given by:

$$\rho_{\parallel} = R_{\parallel}\left(\frac{WH}{L}\right) = R_{\parallel}\left(\frac{V_0}{L^2}\right) \tag{1}$$

and

$$\rho_{\perp} = R_{\perp}\left(\frac{WL}{H}\right) = R_{\perp}\left(\frac{W_0 L}{H_0}\right) \tag{2}$$

By using Eqs. (1) and (2) to calculate resistivity, the volume V_0 was assumed constant, and possible volume changes due to void formation were neglected. Unless indicated otherwise, the parallel resistivity is reported.

3. Results and discussion

3.1. Initial electrical properties

The percolation threshold is a basic characteristic of a conductive composite; in this case the percolation threshold defines the composition range for studying the effect of stretching on conductivity. Fig. 2 shows the variation of the resistivity with the volume fraction of filler. A typical S-shaped curve is observed that separates three regions: insulating, transition, and conductive. The model that is most often used to quantify the changes in the transition and conductive regions is the so-called statistical percolation model [18]. Proposed by Kirkpatrick [19] and Zallen [20], this model predicts the electrical resistivity of an insulator-conductor binary mixture by assuming random positions of the filler particles. The result is a power-law variation of the

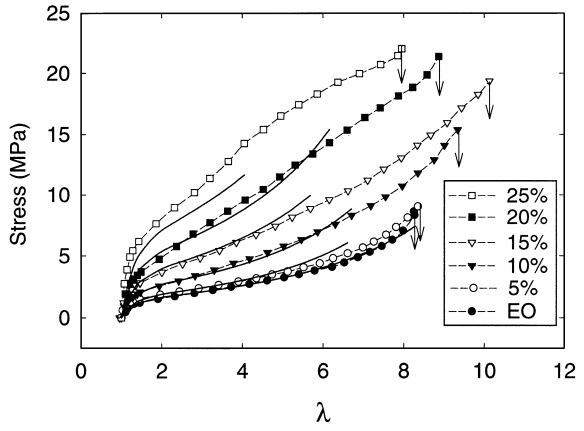

Fig. 3. Mechanical properties of composites with various amounts of carbon black. The solid lines are fits to the slip-link model, Eq. (6), with the shift factor from Eq. (5) for $f = 4.83$.

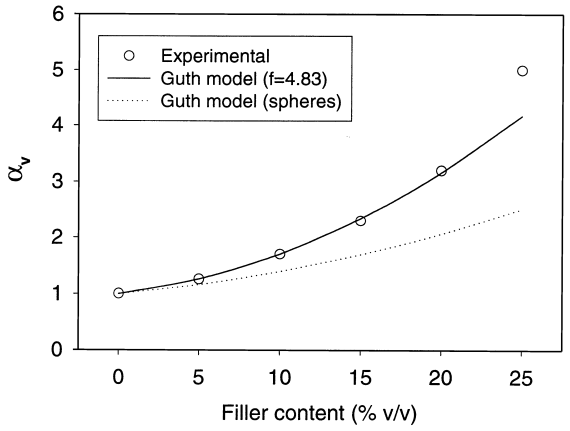

Fig. 5. Comparison of the experimental shift factors with the Guth models for spherical particles (dotted line, Eq. (4)) and rodlike particles (solid line. Eq. (5)).

resistivity ρ, above the percolation threshold:

$$\rho \propto \left(\frac{V - V_c}{1 - V_c}\right)^{-t} \tag{3}$$

where V is the volume fraction of filler, V_c the percolation threshold and t is a universal exponent that is close to 2 for a 3D dispersion [21]. The two-parameter fit is represented in Fig. 2 by the solid line and gives $V_c = 0.12$ and $t = 2.05$. The value of the exponent t is consistent with the model prediction. On the basis of this result, composites with between 12.5 and 30% (v/v) filler were used to study the relationships between resistivity and mechanical deformation. The lower limit was determined by the percolation threshold, the upper limit was the maximum carbon black that could be dispersed in the EO matrix.

A previous study demonstrated that the composite exhibited ohmic behavior before and after stretching to 20% strain [17]. As already indicated [22], this linearity between applied current and measured voltage above the percolation threshold simplifies the analysis and interpretation of the experimental results.

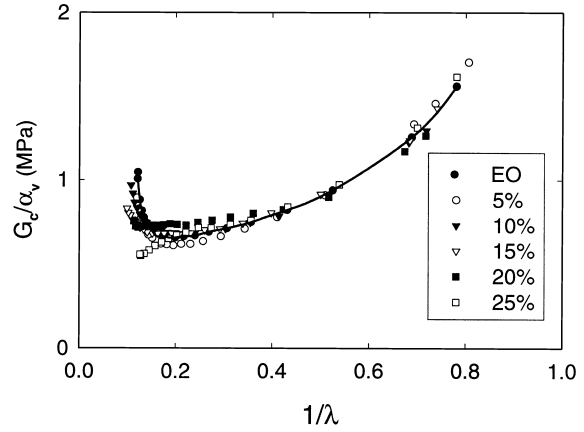

Fig. 4. Rubber modulus $G_c = \sigma(\lambda - 1/\lambda^2)^{-1}$ of composites with various amounts of carbon black, shifted to the rubber modulus G_0 of unfilled EO by a shift factor α_v.

3.2. Mechanical properties

The influence of filler content on the mechanical properties of reinforced-elastomers has been extensively reported in the literature [23]. It is generally agreed that the increase in modulus is due to strong interactions between polymer chains and particles, and/or between particles and particles. Fig. 3 shows the stress–strain curves obtained with various amounts of carbon black dispersed in the EO matrix. By increasing the volume fraction of filler, gradual improvement in modulus and tensile strength was observed. The properties at higher strains were especially impressive. Typically, reinforcement even with high-structure carbon black is accompanied by a decrease in elongation to break [24,25]. This was not the case with the EO composites, which retained the high elongation of the unfilled elastomer even with the maximum filler content of 25% (v/v).

As the stress–strain curves had the same shape as the unfilled EO, it was of interest to compare the reinforcement effect with the Guth hydrodynamic models [26] that are commonly used in the rubber literature. Assuming perfect adhesion between filler and matrix, an important consequence of the Guth analysis is that the stress–strain curves are proportional with the proportionality constant determined by the amount of filler. To test the possibility that the curves would superpose with a simple shift factor, the data are plotted in Fig. 4 as the rubber modulus $G = \sigma(\lambda - 1/\lambda^2)^{-1}$ where λ is the extension ratio and σ is the engineering stress. The curves for the composites were shifted by a factor α_v to obtain the best overlap with the unfilled elastomer. A gradually decreasing modulus at low strains was followed by a region of almost constant modulus. The stress–strain behavior superposed well to about 400% strain. Deviations toward lower modulus values at large

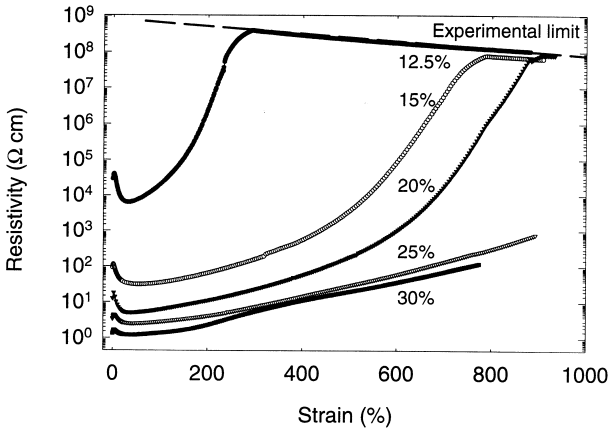

Fig. 6. Influence of carbon black content on the electrical properties under large strain. All carbon black contents are above the percolation threshold.

strains, especially for high-filler contents, were consistent with loss of particle–matrix adhesion.

Fig. 5 is a plot of the shift factors derived from the superposition. The variation of the shift factor with filler volume fraction was smooth and, in particular, there was no transition in the vicinity of the percolation threshold. Therefore the results were compared with Guth reinforcement models [26]. The model for spherical reinforcing particles has the form:

$$G_c = G_0\left(1 + 2.5V + 14.1V^2\right) \tag{4}$$

where G_c and G_0 are the moduli of the composite and matrix, respectively. The linear term accounts for the reinforcing effect of individual particles, and the second power term is the contribution of particle pair interactions. This model significantly underestimates the observed reinforcement, as shown in Fig. 5. The difference between experimental data and Eq. (4) was even observed for a volume fraction as low as 10% (v/v), where the model is most applicable.

An alternative formulation accounts for non-spherical particles. For rodlike particles of aspect ratio f, the reinforcement is given by:

$$G_c = G_0\left(1 + 0.67fV + 1.62f^2V^2\right) \tag{5}$$

Using f as an adjustable parameter, an excellent fit was obtained with $f = 4.83$ for filler contents less than 25% (v/v), Fig. 5. The importance of particle–particle interactions was inferred from the need for the second term in Eq. (5), to describe the mechanical reinforcement. The fit did not hold for a volume fraction of 25% (v/v), probably because the amount of polymer was insufficient to completely wet and disperse the filler. An unsuccessful attempt to disperse more than 30% (v/v) filler supported this hypothesis.

Good agreement of experimental results with Eq. (5) was, however, rather surprising because the model presumably applies only for one parameter stress–strain curves [24], and the mechanical behavior of the EO matrix cannot be described properly by classical rubber theory. Instead, the elastomeric EO copolymer is described by a slip-link model that operates with four parameters [8]: the density of cross-links (N_c), the density of slip-links (N_s), a slippage parameter (η) and an inextensibility parameter (α). The free energy derived from the slip-link theory takes the form:

$$\frac{F}{kT} = \frac{1}{2}N_s\left(\sum_i\left[\frac{\lambda_i^2(1+\eta)(1-\alpha^2)}{\left(1-\alpha^2\sum_i\lambda_i^2\right)(1+\eta\lambda_i^2)} + \log\left(1+\eta\lambda_i^2\right)\right] + \log\left(1-\alpha^2\sum_i\lambda_i^2\right)\right) + \frac{1}{2}N_c\left(\left[\frac{\sum_i\lambda_i^2(1-\alpha^2)}{\left(1-\alpha^2\sum_i\lambda_i^2\right)} + \log\left(1+\eta\lambda_i^2\right)\right] + \log\left(1-\alpha^2\sum_i\lambda_i^2\right)\right) \tag{6}$$

where the summation is made over the Cartesian components of strain. In uniaxial tension, the stress is obtained by:

$$\sigma = \left(\frac{\partial F}{\partial \lambda}\right)_{T,V} \tag{7}$$

The stress–strain behavior of the unfilled matrix was fit with two parameters held constant, $\eta = 1.1$ and $\alpha = 6.5 \times 10^{-2}$. Values for N_c and N_s of 0.37 and 5.76 MPa, respectively, gave the calculated stress–strain curve in Fig. 3, which fit the entire experimental stress–strain curve very well. The calculated curves for the composites were obtained by multiplying the right side of Eq. (6) by the shift factor obtained from Eq. (5) with $f = 4.83$. Good fit with the experimental results extended to high strains, about 500%. The agreement demonstrated that the Guth model can apply for matrices with multiple parameter stress–strain curves. Loss of reinforcement due to extensive damage in the composite at higher strains caused the experimental curve to drop below the calculated one.

3.3. Electrical properties under uniaxial strain

The resistivity as a function of strain for different amounts of filler is displayed in Fig. 6. These curves are separated in four regimes with increasing strain. Regime I is characterized by a sharp increase in resistivity and corresponds to the behavior typically observed with vulcanized rubber composites. It is generally accepted that the increased resistivity is due to breakage of the carbon black network. Regime I ends at a few percent strain in the EO composites. Regime II, extends from the maximum in resistivity at 3–4% strain to about 30% strain. It is characterized

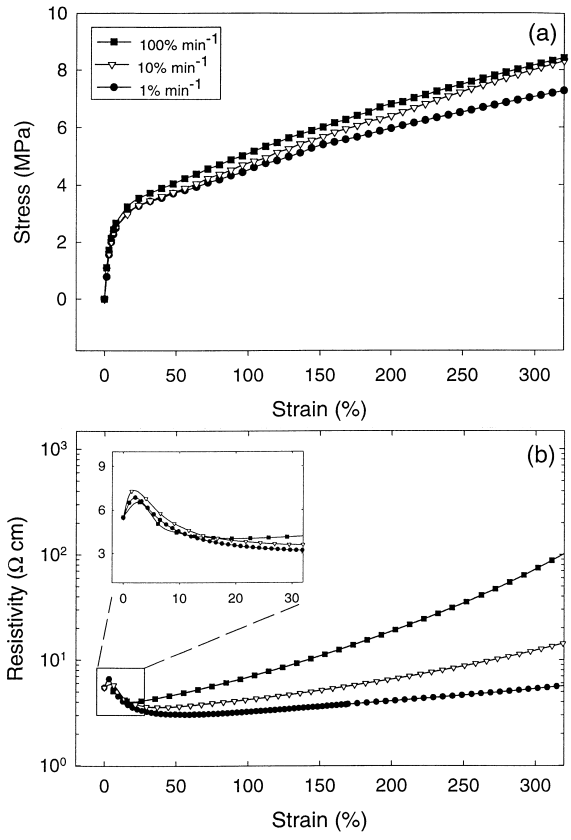

Fig. 7. Effect of strain rate on: (a) mechanical, and (b) electrical properties, of EO with 20%(v/v) carbon black.

by a rapid decrease in the resistivity. This behavior at such a low strain is unusual and has only been observed previously in a few instances [9,27]. In cases where a decrease in resistivity is observed in vulcanized rubber composites, it generally occurs at strains an an order of magnitude higher [29].

In regime III, the resistivity gradually increased. The exponential relationship $\rho \propto \exp(\beta\epsilon)$ where ϵ is the engineering strain, was essentially independent of composition with $\beta = 8 \times 10^{-3}$. This indicated that the filler volume fraction had little influence on the change in resistivity over a very broad range of strain, although the magnitude of the resistivity in regime III decreased with the amount of filler. Regime III ended when the resistivity reached about $10^3\ \Omega$ cm; the corresponding strain increased with the amount of filler. The resistivity at the onset of regime IV corresponded to the percolation transition (Fig. 2). The correlation suggests that the relatively weak conducting network with resistivity about $10^3\ \Omega$ cm can be destroyed either by decreasing the filler volume fraction, or by stretching the composite. Depercolation explained the rapid increase in resistivity upon further stretching. For all volume fractions of filler, growth in resistivity was exponential with a much larger exponent β' than in regime III, $\beta' = 5 \times 10^{-2}$.

Although the electrical response to strain followed the same trends for all compositions, not all the compositions exhibited all four regimes. Thus the composition with 12.5% (v/v) filler, which was close to the percolation threshold, did not exhibit regime III. Also, the composites with the most filler, 25 and 30% (v/v), did not exhibit depercolation, regime IV. The properties in regimes II and III were considered the most interesting, as these differentiated the EO composites from the more widely investigated composites that utilize a vulcanized elastomer matrix. Therefore, the properties in regimes II and III were explored in more depth using a single composition with 20% (v/v) filler.

The effect of strain rate on the stress–strain and resistivity–strain behavior is demonstrated in Fig. 7a and b. The mechanical response of unfilled EO at ambient temperature did not depend on strain rate in this range of strain rates.

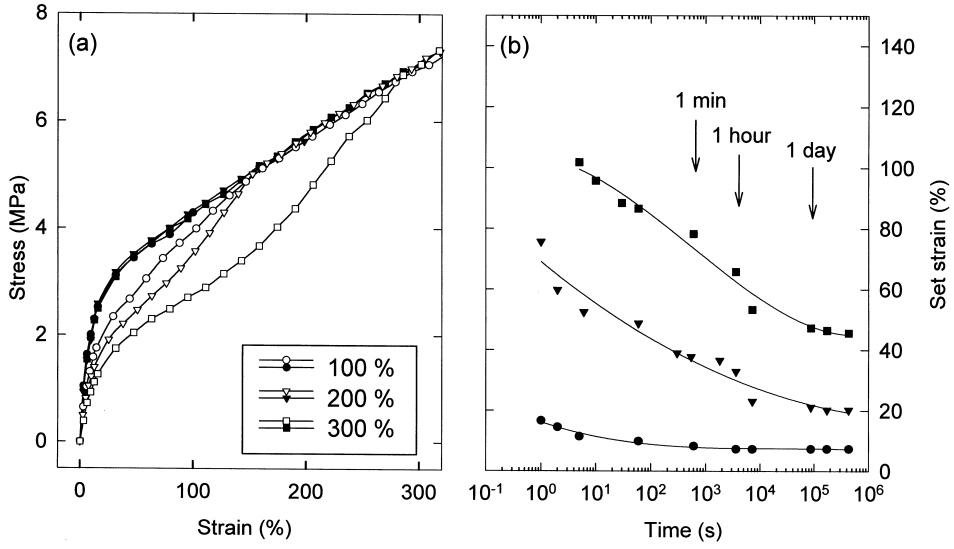

Fig. 8. Effect of pre-strain on: (a) extension, and (b) recovery behavior of EO with 20%(v/v) carbon black, comparing the first (solid symbols) and second (open symbols) extensions.

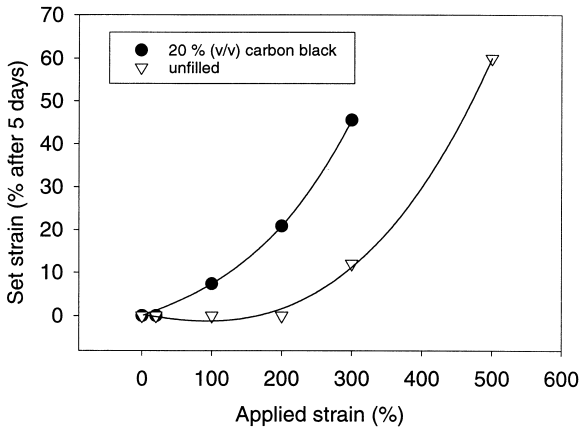

Fig. 9. Influence of 20%(v/v) carbon black on the set strain after five days, compared to the unfilled matrix.

Changing the strain rate by two orders of magnitude also had little effect on the mechanical response of the composites. Regimes I and II in the resistivity–strain behavior were virtually strain-rate independent (inset in Fig. 7b). This observation is of importance for certain applications such as strain gauges. Regime III, on the contrary, showed a strain-rate effect similar to that observed with vulcanized elastomers [22]. Specifically, the parameter that described the exponential dependence of the resistivity gradually increased with strain rate: $\beta \cong 2.5 \times 10^{-3}$, 6.0×10^{-3}, and 1.0×10^{-2} for strain rates 1, 10, and 100% min^{-1}, respectively. Although the electrical response revealed strain-rate dependent changes in the microstructure of the conducting network, these changes did not significantly affect the mechanical response.

3.4. Effect of thermo-mechanical history

The influence of pre-straining the composites into regime III on the mechanical properties is displayed in Fig. 8. Increasing the magnitude of the first strain gradually decreased the stress level on the second extension. The strain-softening, indicating that some breakdown occurred in the composite during the first extension, was similar to the so-called Mullins effect observed with filled vulcanized rubber [1]. In the latter case, the Mullins effect has been attributed either to fracture of chains in the rubber network or to detachment of chains from the surface of the particles during the initial extension. The unfilled EO matrix did not exhibit a Mullins effect when strained to 300%, which made the first explanation unlikely [1]. The second possibility seemed reasonable for these composites.

Although the mechanism was probably different from that proposed for vulcanized rubber, it is suggested that strain-softening of the EO composites was caused by dynamic bonds between particles and matrix. By analogy with Boonstra's interpretation [2], when the composite was subjected to a tensile strain, the shortest or the more strained chain segments between particles rearranged to accommodate the deformation. As a result, the chain length was homogenized and the resistance to elongation was lower on the second extension. Increasing the pre-strain gradually increased the amount of slippage. The higher set strain of the composite compared to the unfilled elastomer was further evidence of physical changes in the microstructure that were not completely reversed by the restoring force of the network, Fig. 9.

Pre-straining the composite to 100% strain did not qualitatively change the electrical response, Fig. 10. A well-defined regime II was observed indicating that the initial microstructure was recovered. However, in composites pre-strained to 200 and 300%, the characteristic decrease in resistivity of regime II was replaced by almost constant resistivity over a broad range of strain. This behavior was interpreted as partial loss of particle–

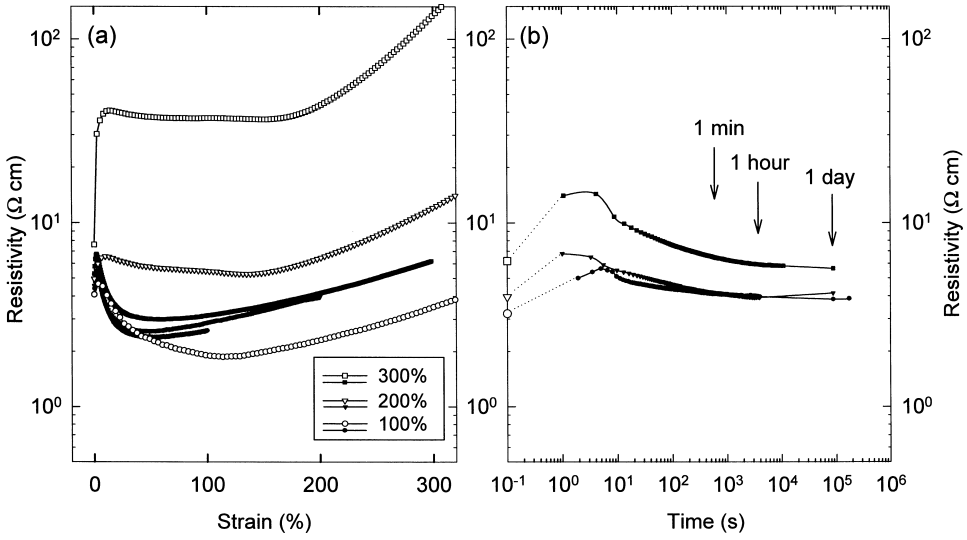

Fig. 10. Effect of pre-strain on the electrical properties of EO with 20%(v/v) carbon black during: (a) extension, (b) recovery, comparing the first (solid symbols) and second (open symbols) extensions.

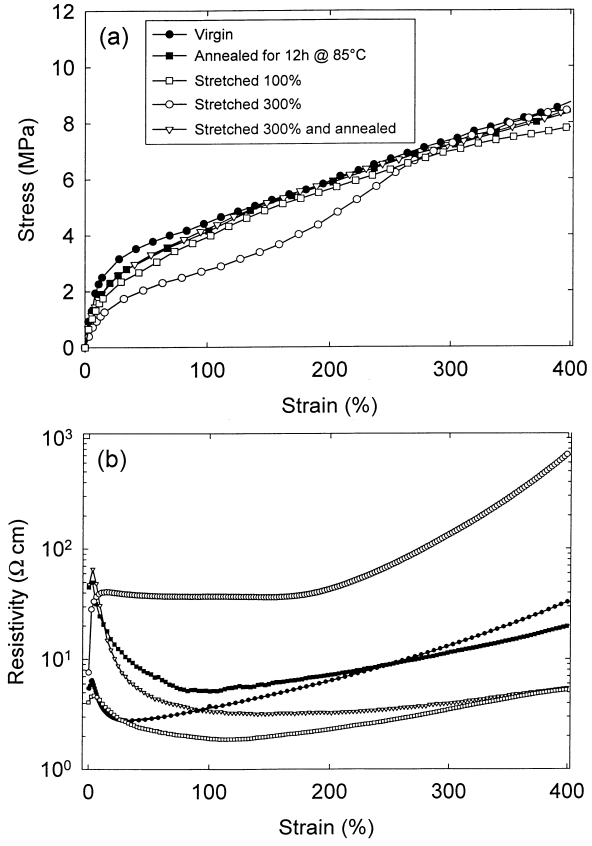

Fig. 11. Effect of thermo-mechanical history on the: (a) mechanical and (b) electrical properties of EO with 20%(v/v) carbon black.

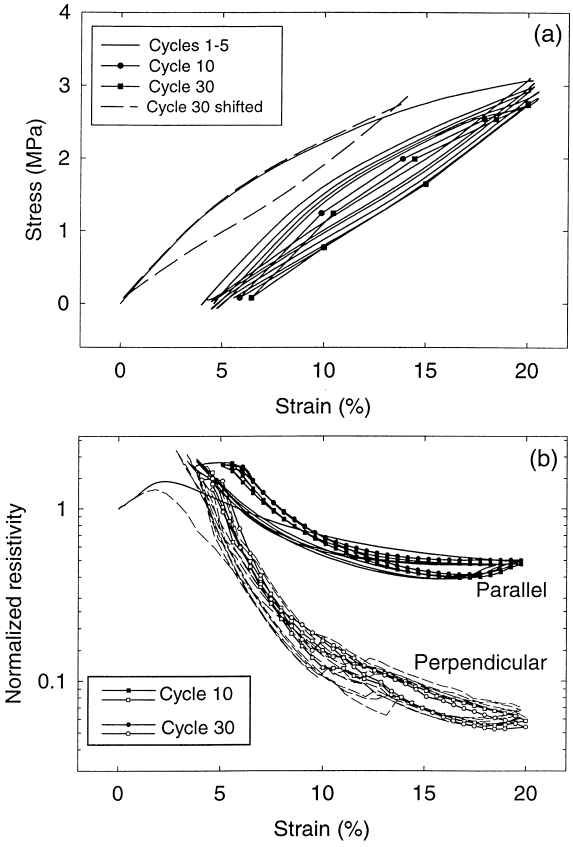

Fig. 12. Effect of cyclic deformation to 20% strain on (a) mechanical, and (b) electrical properties of EO with 20%(v/v) carbon black. $\rho_{0\parallel} = 12$ and $\rho_{0\perp} = 113\ \Omega$ cm.

particle interactions, as already suggested by the Mullins effect. Consequently, the resistivity did not change until the strain was high enough to cause formation of new holes in the percolating network.

The resistivity was also recorded after pre-straining as the unloaded specimen recovered before the second extension, Fig. 10. An initial increase in resistivity confirmed the transient condition of the conducting network at high strains. Similar behavior of carbon black-filled silicone rubber was explained by rapid destruction and reformation of loose contacts between conducting particles [28]. After the initial increase, the slight decrease in resistance was attributed to geometrical changes as the specimen recovered.

Fig. 11a, displays the stress–strain behavior of specimens submitted to different thermo-mechanical histories. Annealing the unstrained composite above the melting range (0–80°C), produced a small decrease in the modulus. Possibly annealing released internal microstresses due to molding. The mechanical behavior of the composite pre-strained to 100% resembled that of the annealed composite. This suggested that at least part of the change in mechanical properties on stretching to 100% was due to relaxation. More interesting was the influence of annealing on the composite after pre-straining to 300%. Although the pre-strained specimen did not quite recover the initial dimensions upon annealing (the set strain dropped from 45 to 15% upon annealing), the strain-softening disappeared and the stress–strain curve was the same as that of the annealed, unstrained composite. As regards the mechanical behavior, annealing above the melting temperature completely erased the strain history.

Regarding the electrical properties, annealing the unstrained composite produced an increase in resistivity suggesting that relaxation of internal stresses during annealing involved particle–particle interactions. The major observation from the resistivity measurements was that annealing the strained composite restored regime II, and therefore erased the damage to the conducting network induced by the mechanical history. The observation that large pre-strains produced both the Mullins effect and the loss of regime II, and that both effects were erased by melting the EO crystals, suggested that they were the mechanical and electrical manifestations, respectively, of the same strain-induced damage to the composite microstructure.

3.5. Cyclic deformation

The stress response to 20% cyclic strain is displayed in Fig. 12a. After the first cycle, the hysteresis was small. The first cycle differed from subsequent cycles due to a transient set strain. Nevertheless, there was no strain-softening even

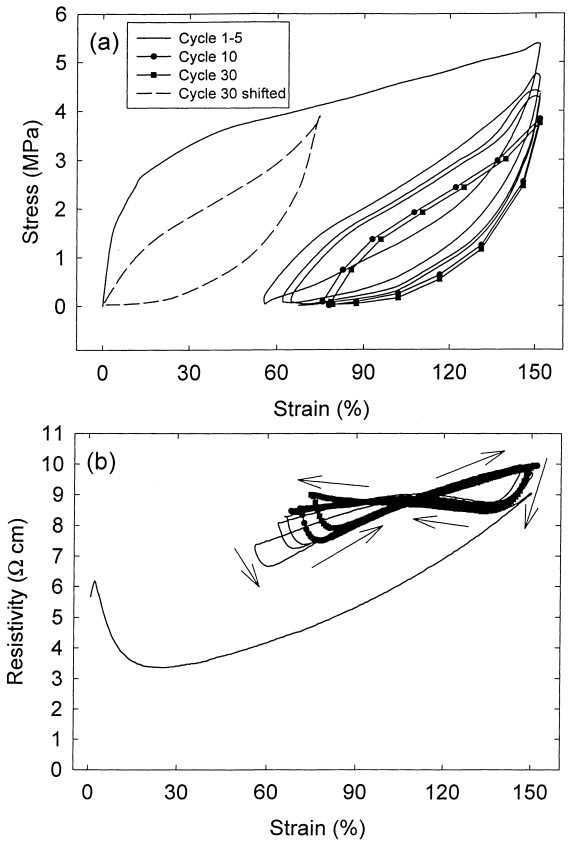

Fig. 13. Effect of cyclic deformation to 150% strain on the: (a) mechanical, and (b) electrical properties of EO with 20%(v/v) carbon black.

on the first cycle as was demonstrated by shifting the 30th cycle to the left on the strain axis to coincide with the 1st loading. The accompanying resistivity exhibited very little hysteresis; all the cycles were very similar. Regime II was entirely reversible; regime I disappeared after the first cycle because the strain set was above the transition from regimes I to II.

The resistivity in the direction perpendicular to the strain, dropped more than the resistivity measured parallel to the strain, Fig. 12b. A decrease in resistivity in the strain direction observed with vulcanized elastomers, at much higher strains, was attributed to particle alignment [29]. The effect of alignment is, however, probably negligible at low strains (below 20%) [16]. Furthermore, the comparison of parallel and perpendicular resistivities, which revealed a larger drop in the perpendicular direction, demonstrated that regime II was not due to particle alignment but to new or improved particle–particle contacts.

Fig. 13 displays the mechanical and electrical response of a specimen cyclically loaded to 150% strain. The first cycle resulted in a large Mullins effect and significant non-recoverable strain. Both the Mullins effect and the strain set increased gradually during subsequent cycles. The large Mullins effect is shown by shifting the 30th cycle along the strain axis to coincide with the 1st cycle. These observations are consistent with the breakdown of particle–matrix interactions in regime III as indicated by the pre-straining experiments.

After the initial loading, the resistivity exhibited hysteresis loops in the shape of a figure eight. The decrease in resistivity upon unloading was due to relaxation of the stretched polymer, which allowed the particles to reform the network. The decrease upon reloading was probably related to the regime II mechanism in the unstretched composite. In between, the resistivity increased slightly on the loading and unloading parts of each cycle. This complex behavior demonstrates the dynamic and time-dependent nature of microstructural changes in regime III.

3.6. Model for EO filled with high-structure carbon black

The four regimes in resistivity of a composite with 20% (v/v) carbon black are shown in Fig. 14. Regime I is generally attributed to network breakage; in the present case, it

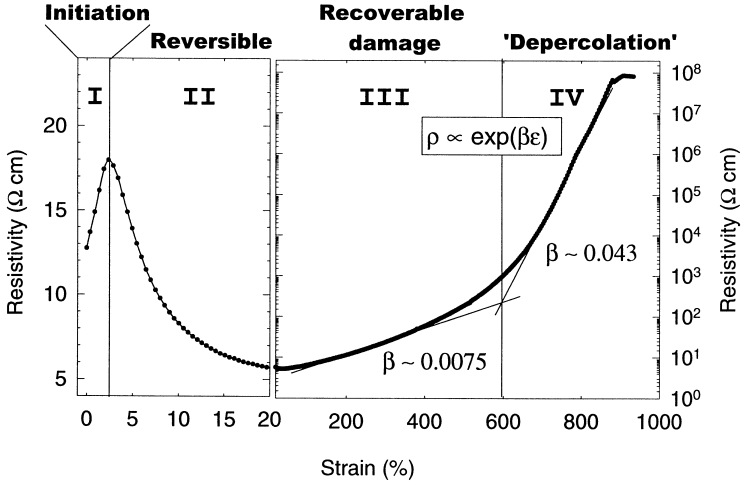

Fig. 14. Definition of the four regimes in the resistivity–strain relationship of EO with 20%(v/v) carbon black.

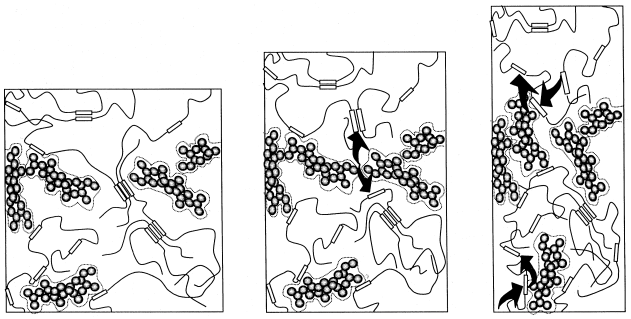

Fig. 15. Schematic representation of the proposed microstructural mechanisms for the decrease in resistivity upon stretching.

can also be considered as an initiation phase for regime II. In regime II, the composite is differentiated from others described in the literature by having virtually no strain rate dependency in the resistivity up to 30% strain. Moreover, in this regime the composite exhibited no permanent strain or irreversible electrical properties during mechanical cycling. These combined properties would make this composite useful as a strain gauge. The primary characteristic of regime III was preservation of the conducting network during deformation to high strains. The properties were recoverable upon rest after straining to 100%. Above 200% strain, the composite did not recover completely upon rest; a Mullins effect also indicated that the composite was damaged. However, the properties were restored by annealing above the melting temperature of the matrix. The mechanistic explanation of regime IV emerged from the percolation curve (Fig. 2). Regime IV, was thought to result from the breakdown of the percolating network, and therefore was called ‘depercolation’.

Using the concept of secondary aggregates [2], regime II could possibly be explained as a reversible rearrangement within the weakly bonded secondary aggregates. In this case, the maximum in resistivity between regimes I and II would be interpreted as the yield strength of the secondary aggregate. Although this mechanism could not be definitively rejected, it is based on the controversial definition of secondary aggregates. Moreover, it assumes that aggregates that were not broken during the rather forceful mixing process could be reversibly deformed during the mild uniaxial extension. Furthermore, this mechanism would not be specific to the EO matrix, and regime II has yet to be reported for carbon black-filled elastomers with permanent cross-links. Finally, this mechanism cannot account for the characteristics of regime III that should, to some extent, be related to regime II.

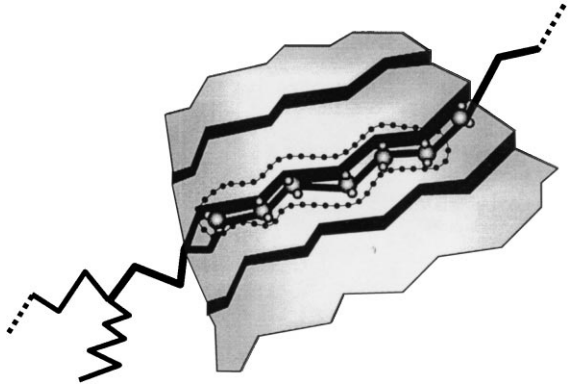

Fig. 16. Schematic representation showing adsorption of a linear EO chain segment to the step-like edges of a carbon black particle, to produce good adhesion.

The EO filled with high-structure carbon black exhibited a combination of properties not generally achievable with this type of filler in an elastomeric matrix, including a decrease in resistivity upon stretching that was reversible up to 20% strain (regime II) and low resistivity with good mechanical properties at high strains (regime III). Furthermore, these characteristics were specific to high-structure carbon black, as composites of the EO elastomer with low-structure carbon black or carbon fibers exhibited more conventional behavior [17]. An explanation appears to require the unique features of both filler and matrix. A possible structural model is presented in Fig. 15. In contrast to a vulcanized elastomer, the concept of a network of flexible chains with fringed micellar crystals serving as the multifunctional junctions provides the structural basis for EO elastomers. A single polymer molecule contains many segments that are long enough to crystallize; these can be incorporated into different crystals to form a network, Fig. 15a.

Upon stretching, the fringed micellar junctions of EO elastomers are not fixed, but are thought to provide a sliding topological constraint by a process of detachment–attachment, which can also be viewed as partial melting [8]. As a result of local stress concentrations, the actual strain in the vicinity of the particle can be several times higher than the average macroscopic strain [30]. Indeed, local strains in regime II may be high enough for crystalline junctions to “melt” and flow out from the space between nearby particles, Fig. 15b. A new electrical pathway is thus created or an existing pathway is improved. The effect should be particularly noticeable in the transverse direction, which contracts during straining due to Poisson’s effect. Recovery is driven by the elastic deformation of the surrounding network of fringed micellar crystals and entanglements. It would seem reasonable that a threshold strain should be observed. The maximum in resistivity between regimes I and II is interpreted as this threshold.

The good mechanical properties and low resistivity in regime III suggest that the system tolerates high strains with very little damage accumulation. It can be imagined that particles incorporated into a network of mobile junctions are less constrained during elongation than those in a network of fixed junctions, and this would facilitate rotation

and translation of aggregates [13,14]. Additionally, at high strains it is necessary to consider the role of particle–matrix adhesion. The embedded carbon black particles adhere strongly to the matrix, as indicated by conformity to the Guth mechanical model. The mode of adhesion is suggested by analogy, to the bound rubber models proposed for vulcanized elastomers [31–33]. Linear chain segments, which are not part of a fringed micellar crystal, are ideal candidates for adsorption to the step-like edges of the carbon black particle, as illustrated in Fig. 16.

Additionally, it is suggested that the particle–matrix bond is dynamic. Although it is imagined that particle–matrix adhesion is not disrupted by the relatively low strains in regime II, higher local stresses in regime III may be sufficient to overcome the physical bond and allow the detached chain to relax closer to the Gaussian state, Fig. 15c. In the process, another chain segment can form a physical bond with the newly created adsorption site, and the damage to the system is minimized. This constitutes a type of "self-healing" mechanism that is unique to EO elastomers. The shortest or most strained chain segments are affected first, and reorganize to increase the connecting length between two particles (lower arrows in Fig. 15c). The dynamic nature of crystal junctions also permits chain segments to melt and adsorb to high-energy sites (upper arrows in Fig. 15c). These irreversible physical changes in particle–matrix adhesion are reflected in the Mullins effect, i.e. the modulus decrease on reloading. The higher set strain of the composite compared to the unfilled elastomer suggests that the restoring force of the network is not sufficient to completely reverse the physical changes. However, the entanglement network almost completely erases the permanent set if the temperature is raised above the crystalline melting point.

In summary, this study focussed on a new elastomer that is a candidate matrix material for conducting composites. The fundamental difference in the network structure of EO elastomers compared to conventional vulcanized rubbers, i.e. multifunctional physical junctions compared to fixed chemical crosslinks, was manifest in the property spectrum achieved with EO composites. Examination of the stress–strain and concurrent resistivity–strain behavior of EO with a high-structure carbon black revealed characteristics that differentiated EO composites from those that utilize more conventional vulcanized rubbers. Particularly interesting was a reversible and strain-rate independent decrease in resistivity up to 30% strain, which could qualify EO composites for strain gauge applications. The properties at higher strains were also impressive. The composites demonstrated modulus reinforcement in accordance with the Guth model for good particle–matrix adhesion. Typically, reinforcement even with high-structure carbon black is accompanied by a decrease in elongation to break. This was not the case with the EO composites, which retained the high elongation of the unfilled elastomer even with the maximum filler content of 25% (v/v). The good high-strain mechanical properties were accompanied by low resistivity. Filler contents of 20–25% (v/v) produced a composite in which the resistivity remained above the percolation threshold, i.e. less than $10^3\ \Omega$ cm, up to fracture at 800–900% strain. Synthesis of the results of various thermo-mechanical treatments led to a microstructural model based on a matrix network of mobile, multifunctional physical junctions, which incorporated a dynamic bond between EO chain segments and high-structure carbon black particles.

Acknowledgements

Numerous stimulating discussions with Dr E.V. Stepanov, CWRU, are gratefully acknowledged. The authors thank J. Chaton and C. Herd of the Columbian Chemicals Company for furnishing the carbon black, and for technical support. This work was generously supported by the Army Research Office (grant DAAG55-98-1-0311) and the National Science Foundation (grant INT-9726537).

References

[1] Kraus G, editor. Reinforcement of elastomers New York: Wiley, 1965.
[2] Boonstra B. In: Morton M, editor. Rubber technology, 2nd ed.. London: Van Nostrand, 1970. p. 51.
[3] Sau KP, Chaki TK, Khastgir D. Polymer 1998;39:6461.
[4] Bhattacharya SK, editor. Metal-filled polymers New York: Dekker, 1986.
[5] Bensason S, Minick J, Moet A, Chum S, Hiltner A, Baer E. J Polym Sci: B: Polym Phys 1996;34:1301.
[6] Bensason S, Nazarenko S, Chum S, Hiltner A, Baer E. Polymer 1997;38:3513.
[7] Bensason S, Nazarenko S, Chum S, Hiltner A, Baer E. Polymer 1997;38:3913.
[8] Bensason S, Stepanov EV, Chum S, Hiltner A, Baer E. Macromolecules 1997;30:2436.
[9] Huang J-C, Huang H-L. J Polym Engng 1997;17:213.
[10] Flandin L, Prasse T, Schueler R, Schulte K, Bauhofer W, Cavaillé J-Y. Phys Rev B 1999;59:14 349.
[11] Carmona F, Barreau F, Delheas P, Canet R. J Phys Lett 1980;40:531.
[12] Miyasaka K, Watanabe K, Jojima E, Aida H, Sumita M, Ishikawa K. J Mater Sci 1982;17:1610.
[13] Narkis M, Ram A, Stein Z. Polym Engng Sci 1981;21:1049.
[14] Yi X-S, Wu G, Ma D. J Appl Polym Sci 1998;67:131.
[15] Flandin L, Cavaillé J-Y, Bréchet Y, Dendievel R. J Mater Sci 1999;34:1753.
[16] Kost J, Foux A, Narkis M. Polym Engng Sci 1994;34:1628.
[17] Flandin L, Chang A, Nazarenko S, Hiltner A, Baer E. J Appl Polym Sci 2000;76:894.
[18] Lux F. J Mater Sci 1993;28:285.
[19] Kirkpatrick S. Rev Mod Phys 1973;45:574.
[20] Zallen R. The physics of amorphous solids. New York: Wiley, 1985 (chap. 4).
[21] Derrida B, Stauffer D, Herrmann HJ, Vannemius J. J Phys Lett 1983;44:701.
[22] Kost J, Foux A, Narkis M. Polym Engng Sci 1983;23:567.
[23] Payne AR. In: Kraus G, editor. Reinforcement of elastomers, New York: Wiley, 1965. p. 94.
[24] Kurian T, De PP, Khastgir D, Tripathy DK, De SK, Peiffer DG. Polymer 1995;36:3875.
[25] Sau KP, Chaki TK, Khastgir D. J Appl Polym Sci 1999;71:887.

[26] Guth E. J Appl Phys 1945;16:20.
[27] Shui X, Chung DDL. Smart Mater Struct 1997;6:102.
[28] Kost J, Foux A, Narkis M. J Appl Polym Sci 1984;29:3937.
[29] Norman RH. Conductive rubbers and plastics. Amsterdam: Elsevier, 1970.
[30] Fukahori Y, Seki W. J Mater Sci 1994;29:2767.
[31] Donnet J-B. Carbon 1994;32:1305.
[32] Karasek L, Sumita M. J Mater Sci 1996;31:281.
[33] Leblanc JL. J Appl Polym Sci 1997;66:2257.